Supplementary Information for

Modulating Leidenfrost-like Prompt Jumping of Sessile Droplets on Microstructured Surfaces

Wenge Huang [a], Lei Zhao [b,*], Yang Li [a], Xukun He [a], C. Patrick Collier [c], Zheng Zheng [d], Jiansheng Liu [d], Jiangtao Cheng [a,*]

[a] Department of Mechanical Engineering, Virginia Tech, Blacksburg, VA 24061, USA

[b] State Key Laboratory of High-performance Precision Manufacturing, Dalian University of Technology, Dalian 116024, PR China

[c] Center for Nanophase Materials Sciences, Oak Ridge National Laboratory, Oak Ridge, TN 37831, USA

[d] School of Electronic and Information Engineering, Beihang University, 37 Xueyuan Road, Beijing 100191, China

*Corresponding author: Lei Zhao leizhao@dlut.edu.cn

Jiangtao Cheng chengjt@vt.edu

This file includes:

Supplementary Figs. 1 to 8

Supplementary Discussions 1 to 4

Supplementary Table 1

Supplementary Movie Description

Supplementary References

Supplementary Figures

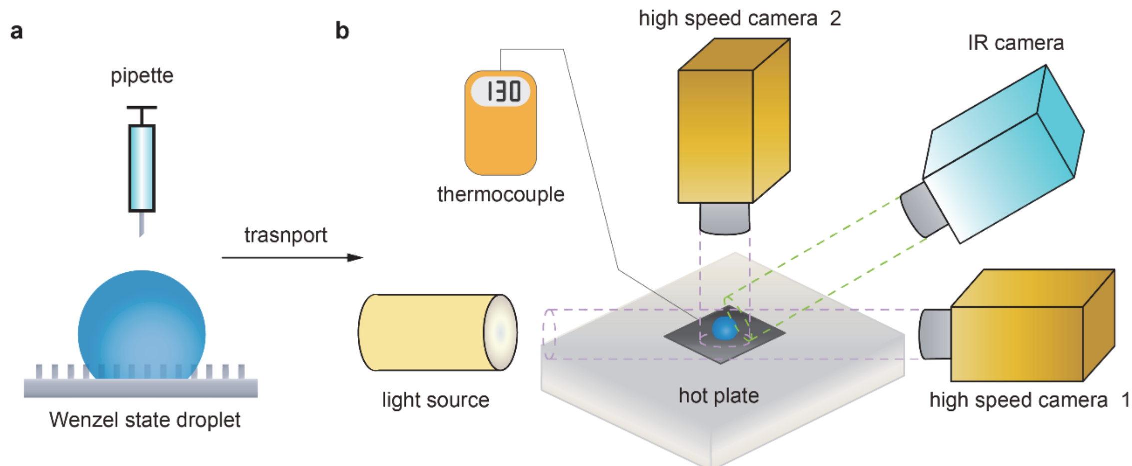

Supplementary Figure. 1 Experimental setup for the Leidenfrost-like droplet jumping study. **a** A water droplet is initially deposited on the micropillared substrate in Wenzel state and then both the droplet and the substrate are carefully translated to a hot plate preheated at 130 °C. **b** Experimental setup for droplet jumping observation. The temperature of the substrate is measured by a K-type thermocouple embedded in the hot plate underneath the substrate. Surface temperature of the droplet is monitored by an IR camera (FLIR A655sc) after moving the substrate on the hot plate. The vibration and jumping processes of the boiling droplet are recorded by a side view high-speed camera (nac MEMRECAM HX-3) and the vapor bubble growth process is monitored by another high-speed camera from the top (Photron FASTCAM SA-6).

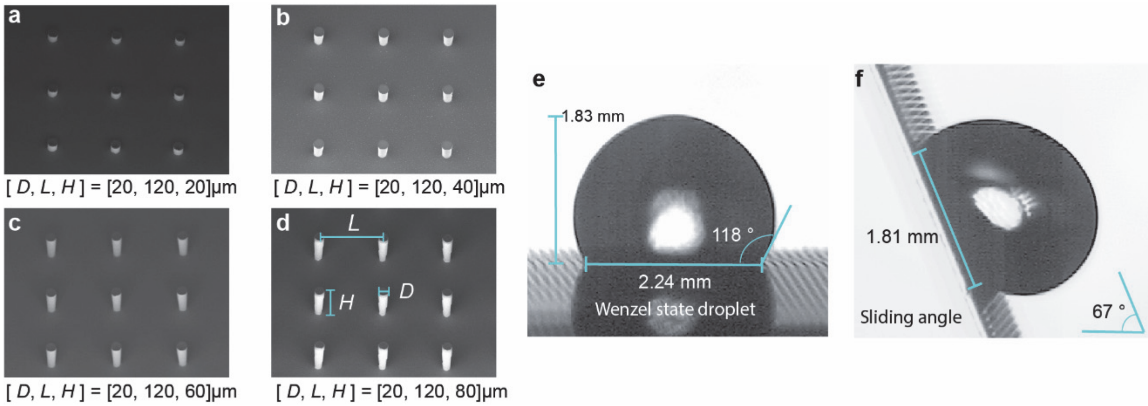

Supplementary Figure. 2 Substrate topology details of the engineered surfaces used in this study. a The scanning electron micrography (SEM) of substrate $[D,\ L,\ H] = [20, 120, 20]$μm. **b** SEM image of substrate $[D,\ L,\ H] = [20, 120, 40]$μm. **c** SEM image of substrate $[D,\ L,\ H] = [20, 120, 60]$μm. **d** SEM image of substrate $[D,\ L,\ H] = [20, 120, 80]$μm. **e** Wenzel state droplet on substrate $[D,\ L,\ H] = [20, 120, 80]$μm at room temperature. The height of the sessile droplet is 1.83 mm; the contact diameter of the droplet is 2.24 mm; the contact angle of the droplet is 118°. **f** Sliding angle of the droplet on the substrate $[D,\ L,\ H] = [20, 120, 80]$μm at room temperature is 67°.

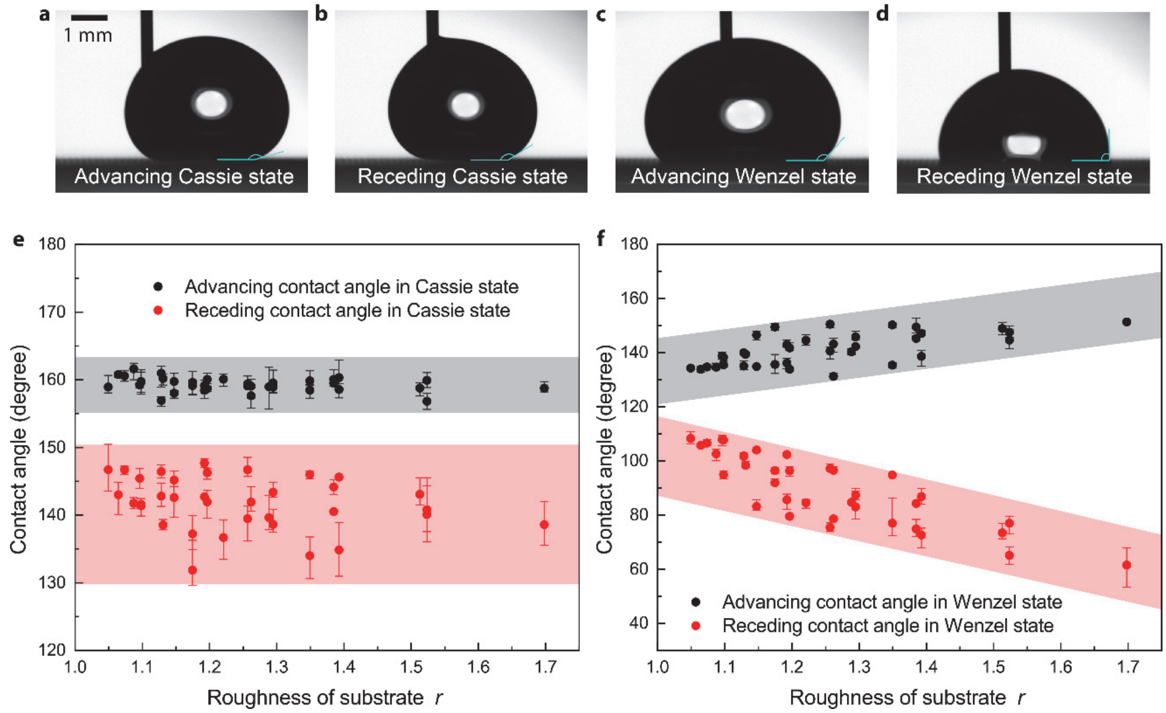

Supplementary Figure. 3 Droplet contact angles on the engineered substrates. **a** Schematic of advancing contact angle (ACA) measurement in Cassie state on the micropillared substrate $[D,\ L,\ H] = [20, 120, 20]\mu\text{m}$. **b** Schematic of receding contact angle (RCA) measurement in Cassie state on the micropillared substrate $[D,\ L,\ H] = [20, 120, 20]\mu\text{m}$. **c** Schematic of advancing contact angle measurement in Wenzel state on the micropillared substrate $[D,\ L,\ H] = [20, 120, 20]\mu\text{m}$. **d** Schematic of receding contact angle measurement in Wenzel state on the micropillared substrate $[D,\ L,\ H] = [20, 120, 20]\mu\text{m}$. **e** Relationship between the substrate roughness r and the ACA/RCA of droplets in the Cassie state. **f** Relationship between the substrate roughness r and the ACA/RCA of droplets in the Wenzel state.

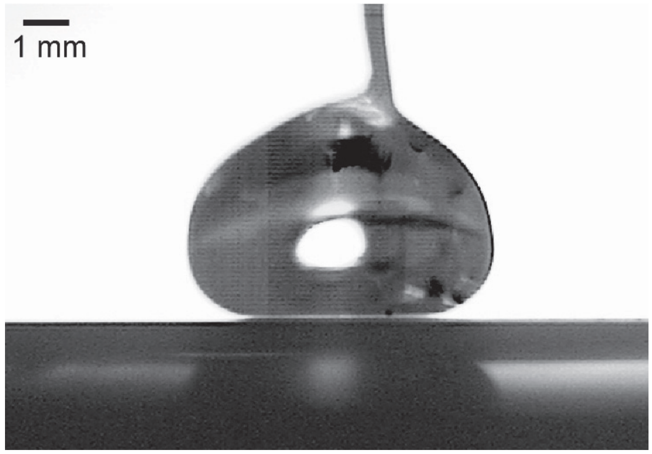

Supplementary Figure. 4 Droplet in the Leidenfrost state on the micropillared substrate. Snapshot of droplet in the Leidenfrost state on substrate $[D,\ L,\ H] = [20, 120, 80]$μm at 330 °C.

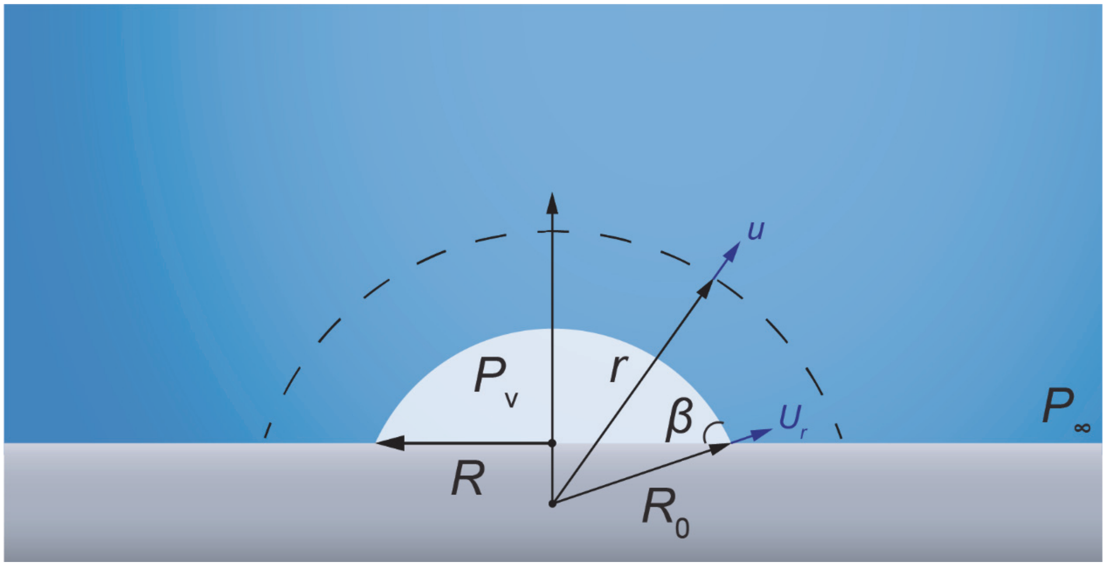

Supplementary Figure 5. Diagram of vapor bubble expansion via momentum interaction with the surrounding liquid at the droplet base.

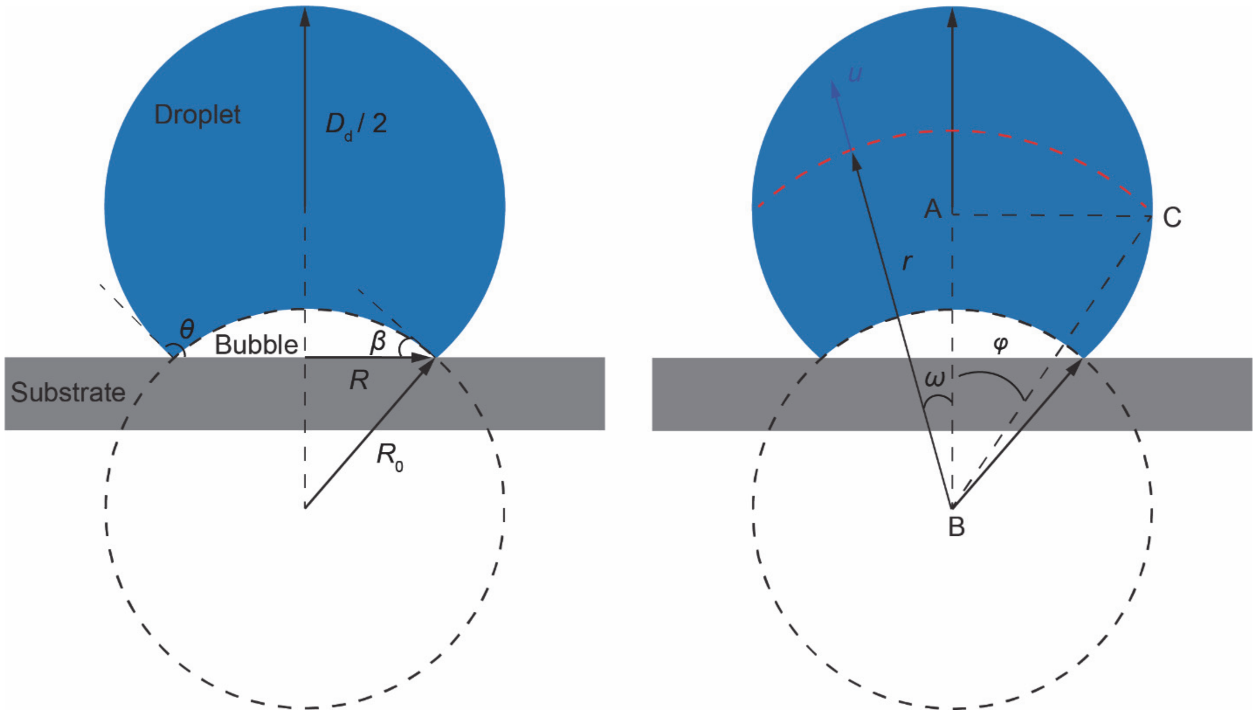

Supplementary Figure 6. Diagram of bubble-droplet geometry when the droplet is about to jump off the substrate.

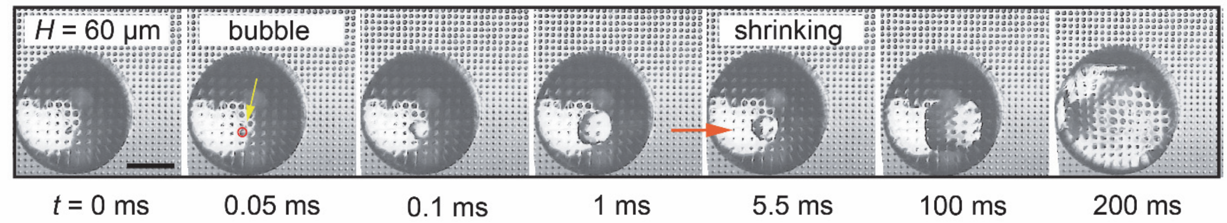

Supplementary Figure 7. Top-view snapshots of vapor bubble growth on substrate $[\boldsymbol{D},\ \boldsymbol{L},\ \boldsymbol{H}] = [\mathbf{20}, \mathbf{120}, \mathbf{60}]$ μm at 130°C.

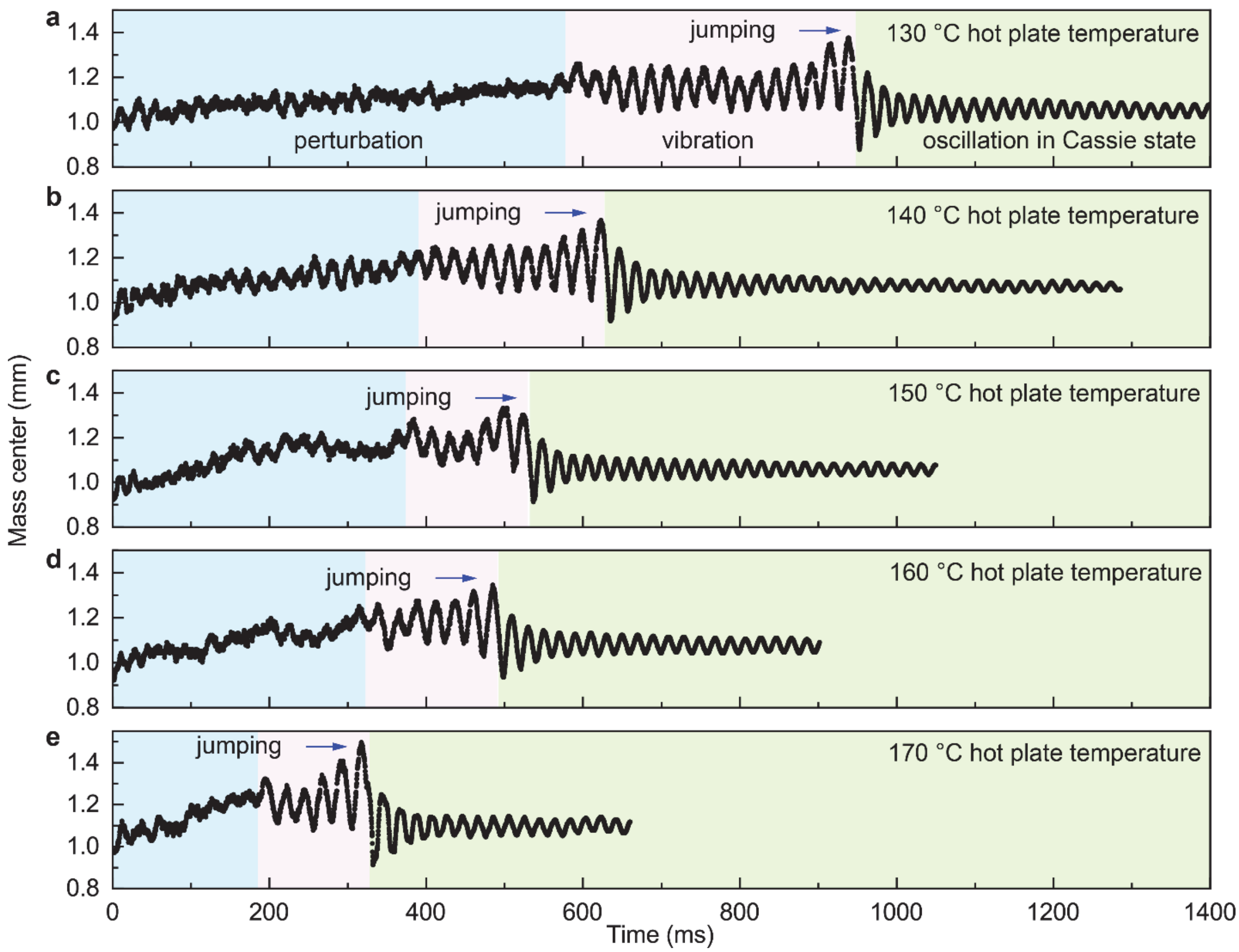

Supplementary Figure 8. Droplet mass center variation on the hot substrate $[\boldsymbol{D},\ \boldsymbol{L},\ \boldsymbol{H}] = [\mathbf{20}, \mathbf{120}, \mathbf{20}]\,\boldsymbol{\mu}\mathbf{m}$ at different temperatures. **a** Droplet height variation on substrate at 130 °C. **b** Droplet height variation on substrate at 140 °C. **c** Droplet height variation on substrate at 150 °C. **d** Droplet height variation on substrate at 160 °C. **e** Droplet height variation on substrate at 170 °C.

Supplementary Discussion 1: Contact angle on microstructured substrates

It can be seen in Fig. S2e that, for droplets in Cassie state, both the advancing contact angle (ACA) and the receding contact angle (RCA) are almost independent of the substrate roughness. In this study, the increase of the substrate roughness $r = \frac{L^2+\pi DH}{L^2}$ is mainly caused by the increase of the micropillar height H. The Cassie state droplet resides only on the tips of the micropillars and as a result, the increase of the substrate roughness r has no obvious influence on the Cassie state droplet's ACA and RCA.

However, it is observed in Fig. S2f that the ACA of droplet in Wenzel state increases with the increase of the substrate roughness and the RCA of the droplet in Wenzel state decreases with the increase of the substrate roughness. The increase of the micropillar height (increase of the substrate roughness) leads to the increase of the adhesion between the Wenzel state droplet and the substrate. Thus, it requires a larger ACA or a smaller RCA to generate a sufficient depinning force to actuate the pinned droplet.

ACA and RCA of droplets in both Cassie state and Wenzel state have been measured and are listed in Supplementary Table 1. To measure the ACA, the droplet was deposited on the substrate with a syringe needle inserted in to the droplet body from the top. Water was slowly and steadily pumped into the droplet to gradually increase the droplet volume. Simultaneously, the droplet's contact angle continuously increased while its contact line kept pinned. The transient contact angle was recorded as the ACA when the initially pinned contact line started to move. The opposite was done to measure the RCA: water liquid was pumped out from the droplet and the transient contact angle was recorded as the RCA when the droplet's contact line started to shrink. It is noteworthy that the RCA usually depends on the size of the droplet. The measured RCA might not be accurate when the sessile droplet volume is too small. Korhonen *et al.*[1] proposed a reasonable lower limit of 5 μL for the droplet volume in order to measure a reliable RCA of a sessile water droplet. Thus, in this study, all the RCAs were measured with droplet volume larger than 5 μL.

Supplementary Discussion 2: Rayleigh-Plesset equation

As demonstrated in Fig. S5, U_r is the radial velocity of the expanding bubble interface with spherical radius R_0. Considering the radial waterflow around the vapor bubble that follows the continuity equation $\frac{\partial r^2 u}{\partial r} = 0$, the radial waterflow velocity u at arbitrary coordinate r in the liquid domain can be calculated as $u = U_r \frac{R_0^2}{r^2}$. Then the kinetic energy of the water domain caused by the expansion bubble can be calculated as:

$$KE = \frac{1}{2}\rho_{\mathrm{l}} \int_{R_0}^{R_d} u^2 \cdot 2\pi r^2 (1 - \cos\beta) dr \tag{S1}$$

where R_d is the radius of the droplet and we consider the bubble size is much smaller than the droplet size $R_d \gg R_0$.

The vaporization-induced bubble overpressure drives the receding of the surrounding liquid. The net work done against the surrounding liquid as the bubble grows from $r = 0$ to R_0 is given by:

$$W = \int_0^{R_0} \left(P_v - P_\infty - \frac{2\sigma}{r}\right)\left(2\pi r^2 (1 - \cos\beta)\right) dr \tag{S2}$$

The energy stored inside the vapor bubble with overpressure is then converted into the kinetic energy of the water droplet, so we have $KE = W$. Thus, we obtain:

$$(1 - \cos\beta)\pi\rho_{\mathrm{l}} \left(\frac{dR_0}{dt}\right)^2 R_0^3 = \left(P_v - P_\infty - \frac{2\sigma}{R}\right) 2\pi(1 - \cos\beta)\frac{R_0^3}{3} \tag{S3}$$

Then differentiating the entire equation with respect to R_0, the Rayleigh-Plesset equation is obtained:

$$\rho_{\mathrm{l}} R_0 \ddot{R}_0 + \rho_{\mathrm{l}} \frac{3\dot{R}_0^2}{2} = \left(P_v - P_\infty - \frac{2\sigma}{R}\right) \tag{S4}$$

Assuming the constant contact angle β during the bubble expanding process, we can express the bubble contact radius as $R = R_0 \sin\beta$. As a result, the Rayleigh-Plesset equation with respect to the bubble contact radius is obtained:

$$\rho_{\mathrm{l}} R \ddot{R} + \rho_{\mathrm{l}} \frac{3\dot{R}^2}{2} = \left(P_v - P_\infty - \frac{2\sigma}{R}\right)\sin^2\beta \tag{1}$$

The inertia-controlled bubble expansion can be divided into two stages by considering the variation of the overpressure. In the first stage, the pressure term on the right-hand-side of the equation is assumed to be constant considering the constant substrate superheat $P_v - P_\infty - \frac{2\sigma}{R} \approx \left(\frac{\Delta T}{T_{\mathrm{sat}}(P_{\mathrm{a}})}\right) h_{\mathrm{lv}}\rho_{\mathrm{v}}$. Multiplying both sides of the equation with $2R^2\dot{R}$, we can get the differential form as:

$$d\left(\rho_{\mathrm{l}} R^3 \dot{R}^2\right)/dt = d\left[\frac{2R^3}{3}\left(\frac{\Delta T}{T_{\mathrm{sat}}(P_{\mathrm{a}})}\right)\frac{h_{\mathrm{lv}}\rho_{\mathrm{v}}}{\rho_{\mathrm{l}}}\sin^2\beta\right]/dt \tag{S5}$$

Then we do the time integration from 0 to t for the equation in the first stage:

$$\int_0^t \frac{d(\rho_l R^3 \dot{R}^2)}{dt} dt = \left(\frac{\Delta T}{T_{\text{sat}}(P_a)}\right) \frac{h_{lv}\rho_v}{\rho_l} \sin^2\beta \int_0^t \frac{d(2R^3)}{3dt} dt \tag{S6}$$

With the temporal boundary condition $R(t = 0) = 0$, we obtain the analytical solution for the vapor bubble contact radius $R(t)$:

$$R^3\dot{R}^2 = \frac{2}{3}\left(\frac{\Delta T}{T_{\text{sat}}(P_a)}\right) \frac{h_{lv}\rho_v}{\rho_l} \sin^2\beta\, R^3 \tag{S7}$$

Then the contact radius in the first stage can be solved as:

$$R\,(t) = \left[\frac{2}{3}\left(\frac{\Delta T}{T_{\text{sat}}(P_a)}\right) \frac{h_{lv}\rho_v}{\rho_l}\right]^{\frac{1}{2}} \sin\beta \cdot t \tag{2}$$

During the second stage, the overpressure of the vapor bubble decreases to zero $P_v - P_\infty - \frac{2\sigma}{R} \approx 0$. And the equation reduces to the inertia form: $\rho_l R\ddot{R} + \rho_l \frac{3\dot{R}^2}{2} = \frac{d}{dt}(\rho_l R^3 \dot{R}^2) = 0$. Then we integrate the differential form of the equation in the second stage. Assuming the first stage sustains between 0 to $t_1 = 0.1\ ms$ and the second stage start from t_1 with the bubble contact radius $R(t = t_1) = R_1$, we get:

$$\int_{t_1}^t \frac{d}{dt}(\rho_l R^3 \dot{R}^2) dt = 0 \tag{S8a}$$

$$R^{3/2}\dot{R} = R_1^{3/2}\dot{R}_1 \tag{S8b}$$

here $R^{\frac{3}{2}}\dot{R}$ is the differential form of $\frac{d}{dt}(R^{5/2})$, we get:

$$\int_{t_1}^t \frac{d}{dt}(R^{5/2}) dt = R_1^{3/2}\dot{R}_1(t - t_1) \tag{S9a}$$

$$R^{5/2} = R_1^{3/2}\dot{R}_1(t - t_1) + R_1^{5/2} = R_1^{3/2}\dot{R}_1\left(t - t_1 + \frac{R_1}{\dot{R}_1}\right) \tag{S9b}$$

As a result, we have:

$$R = \left[R_1^{3/2}\dot{R}_1\left(t - t_1 + \frac{R_1}{\dot{R}_1}\right)\right]^{0.4} \tag{S10}$$

We can also approximate R_1 from the above equation by taking $\frac{R_1}{\dot{R}_1} \approx t_1$ so that R during the second stage can be scaled as:

$$R = \left(R_1^{3/2}\dot{R}_1\, t\right)^{0.4} \sim t^{0.4} \tag{S11}$$

Supplementary Discussion 3: Upward momentum calculation

We here calculate the upward momentum as the droplet is about to detach from the substrate. In this scenario (as depicted in Fig. S6), the vapor bubble has a spherical radius of R_0 and a contact radius of R on the substrate. The apparent contact angle of the vapor bubble on the substrate is β, which relates the spherical radius and the contact radius as $R = R_0\sin\beta$. Simultaneously, the water droplet maintains a constant diameter of D_d (equivalent to a radius of $\frac{D_\mathrm{d}}{2}$) and a contact angle of θ on the substrate. The contact angles for both the vapor bubble (β) and the water droplet (θ) are essentially determined by the same Yang-Laplace equation at the three-phase contact line. Thus, the vapor bubble's contact angle β is approximately the supplementary angle of the water droplet's contact angle θ, which means that $\beta + \theta \approx \pi$. With the relationship established between these two contact angles, the vapor bubble's spherical radius R_0 is equal to the radius of the water droplet, *i.e.*, $R_0 = \frac{D_\mathrm{d}}{2}$.

Now, assuming that the isotropic expansion of the vapor bubble leads to the radial water flow away from the bubble, we apply the continuity equation $\frac{\partial r^2 u}{\partial r} = 0$ where u is the radial water flow velocity and r is the radial coordinate of the droplet domain as shown in Fig. S6. Given the expansion velocity at the vapor bubble interface, denoted as $\dot{R}_0$, we can calculate the radial water flow velocity, u, at any position r inside the droplet using the equation: $u = \frac{\dot{R}_0 R_0^2}{r^2}$.

Subsequently, we determine the component of the radial water flow velocity in the z-axis direction as $U_r\cos\omega$. The upward equivalent momentum can then be calculated by integrating with the mass of the entire droplet. At the moment when the droplet is about to detach, the z-momentum of the water droplet can be expressed as an integral:

$$M_z = \rho_\mathrm{l} \int_{R_0}^{\frac{D_\mathrm{d}}{2}+2R_0\cos\beta} dr \ \cdot \int_0^{\varphi} (u\cos\omega)\cdot(2\pi r\sin\omega)\cdot(r d\omega) \qquad \text{(S12)}$$

Note that φ is the angle in the triangle ABC and can be expressed as:

$$\cos\varphi = \frac{AB^2+BC^2-AC^2}{2AB\cdot BC} = \frac{(2R_0\cos\beta)^2+r^2-R_0^2}{4rR_0\cos\beta} \qquad \text{(S13)}$$

As a result, z-momentum of the water droplet can be simplified as:

$$M_z = 2\pi\rho\dot{R}_0R_0^2 \int_{R_0}^{R_0(1+2\cos\beta)} dr \ \cdot \int_0^{\varphi} \sin\omega\cdot\cos\omega\cdot d\omega \qquad \text{(S14)}$$

Considering that

$$\int_0^{\varphi} \sin\omega\cdot\cos\omega\cdot d\omega = -\frac{1}{4}\int_0^{\varphi} d\big(\cos(2\omega)\big) = \frac{1}{4}\big(1-\cos(2\varphi)\big) = \frac{1}{2}(1-\cos^2\varphi) \qquad \text{(S15)}$$

$$M_z = 2\pi\rho\dot{R}_0 R_0^2 \int_{R_0}^{R_0(1+2\cos\theta)} \frac{1}{2}(1-\cos^2\varphi)dr \tag{S16}$$

$$\frac{1}{2}(1-\cos^2\varphi) = \frac{1}{2}\left[1-\frac{(2R_0\cos\beta)^2+r^2-R_0^2}{4rR_0\cos\beta}\right]\cdot\left[1+\frac{(2R_0\cos\beta)^2+r^2-R_0^2}{4rR_0\cos\beta}\right] \tag{S17}$$

$$M_z = \pi\rho\dot{R}_0 R_0^2 \int_{R_0}^{R_0(1+2\cos\theta)} \left[1-\frac{(2R_0\cos\beta)^2+r^2-R_0^2}{4rR_0\cos\beta}\right]\cdot\left[1+\frac{(2R_0\cos\beta)^2+r^2-R_0^2}{4rR_0\cos\beta}\right]dr \tag{S18}$$

Thus, we obtain:

$$M_z = \frac{(4-3\cos\beta)\cos\beta\pi\rho_l\dot{R}R^3}{3\sin^4\beta} \tag{S19}$$

And the propulsive force is then evaluated by taking the time differentiation of the droplet momentum:

$$F_z \approx \frac{(4-3\cos\beta)\cos\beta\pi\rho_l R^2\dot{R}^2}{\sin^4\beta} \tag{4}$$

Supplementary Discussion 4: COMSOL simulation setup

Fig. 5b depicts the simulated temperature distribution in water droplet on the micropillared substrates by COMSOL® 5.6. In the simulation, a small control volume spanning 2 pillars horizontally and extending 120 μm into the water domain was considered, with the substrate temperature set at 130 °C. The control volume's side surface was assigned periodic boundary conditions to account for the repetitive pillars. The simulation captured the temperature distribution at 10 ms after substrate heating, significantly longer than the bubble expansion time (1.32 ms). Utilizing COMSOL® computation, we obtained the normal total heat flux from the substrate. For the substrate with 20 μm micropillars, the normal heat transfer rate was calculated as $q = 0.41\,W$. Consequently, the heat flux at the droplet base was estimated as $q'' = \frac{q}{\pi R^2} \approx 127\,\mathrm{kW}/m^2$. For the substrate with 80 μm micropillars, the normal heat transfer rate was determined as $q = 0.61\,W$, resulting in an estimated heat flux at the droplet base of $q'' = \frac{q}{\pi R^2} \approx 190\,\mathrm{kW}/m^2$.

Supplementary Table 1. Experimental values of advancing contact angle (ACA) and receding contact angle (RCA) on the silicon-based micropillared substrates used in this study.

Specifications	**Cassie state ACA (°)**	**Cassie state RCA (°)**	**Wenzel state ACA (°)**	**Wenzel state RCA (°)**
$[D, L, H]$ = [20, 120, 20] μm	161±2	141±1	135±2	103±2
$[D, L, H]$ = [20, 120, 40] μm	160±2	138±3	136±4	92±2
$[D, L, H]$ = [20, 120, 60] μm	158±2	139±3	131±2	78±2
$[D, L, H]$ = [20, 120, 80] μm	158±2	146±1	135±2	77±9
$[D, L, H]$ = [20, 140, 20] μm	161±1	143±3	134±2	106±1
$[D, L, H]$ = [20, 140, 40] μm	161±3	146±1	135±2	102±4
$[D, L, H]$ = [20, 140, 60] μm	159±2	148±1	136±3	86±4
$[D, L, H]$ = [20, 140, 80] μm	159±1	147±2	141±3	75±2
$[D, L, H]$ = [20, 160, 20] μm	159±2	147±4	134±1	108±2
$[D, L, H]$ = [20, 160, 40] μm	160±2	141±2	136±2	95±3
$[D, L, H]$ = [20, 160, 60] μm	160±2	145±2	135±1	83±2
$[D, L, H]$ = [20, 160, 80] μm	159±1	146±1	134±2	80±3
$[D, L, H]$ = [30, 120, 20] μm	160±1	139±1	139±1	98±1
$[D, L, H]$ = [30, 120, 40] μm	159±2	142±3	143±1	97±2
$[D, L, H]$ = [30, 120, 60] μm	159±2	135±4	139±1	73±2
$[D, L, H]$ = [30, 120, 80] μm	157±2	140±5	148±1	77±5
$[D, L, H]$ = [30, 140, 20] μm	159±1	145±2	139±1	108±4
$[D, L, H]$ = [30, 140, 40] μm	158±2	143±1	143±4	102±3
$[D, L, H]$ = [30, 140, 60] μm	159±4	140±4	140±4	85±1
$[D, L, H]$ = [30, 140, 80] μm	160±1	144±2	145±3	75±1
$[D, L, H]$ = [30, 160, 20] μm	161±1	147±1	135±2	107±4
$[D, L, H]$ = [30, 160, 40] μm	158±1	143±3	147±2	104±3
$[D, L, H]$ = [30, 160, 60] μm	160±2	137±3	145±2	85±3
$[D, L, H]$ = [30, 160, 80] μm	160±2	143±2	142±1	83±6
$[D, L, H]$ = [40, 120, 20] μm	159±2	132±5	149±2	96±2
$[D, L, H]$ = [40, 120, 40] μm	160±2	134±4	160±2	102±1
$[D, L, H]$ = [40, 120, 60] μm	160±2	121±5	145±4	65±4
$[D, L, H]$ = [40, 120, 80] μm	159±1	139±4	151±1	62±8
$[D, L, H]$ = [40, 140, 20] μm	157±1	143±2	140±1	102±2
$[D, L, H]$ = [40, 140, 40] μm	159±2	139±4	150±2	97±2
$[D, L, H]$ = [40, 140, 60] μm	160±2	141±1	149±4	84±1
$[D, L, H]$ = [40, 140, 80] μm	159±2	143±3	149±3	73±4
$[D, L, H]$ = [40, 160, 20] μm	160±2	142±1	138±1	108±1
$[D, L, H]$ = [40, 160, 40] μm	160±2	142±3	142±2	96±3
$[D, L, H]$ = [40, 160, 60] μm	159±1	139±3	146±2	88±3
$[D, L, H]$ = [40, 160, 80] μm	160±3	146±1	147±2	87±4

Supplementary Movies Description

Movie S1

Leidenfrost-like jumping droplet on micropillared substrates at 130 °C.

Side-view video of the Leidenfrost-like jumping droplet shown in Fig. 1a. Water droplet of 2 mm in diameter resting on substrate $[D,\ L,\ H] = [20, 120, 80]$μm explosively jumps off the substrate in milliseconds.

Movie S2

Vapor bubble expansion process on hot substrate with 80 μm micropillars.

Top-view video of the rapid vapor bubble expansion for the Leidenfrost-like jumping droplet on substrate $[D,\ L,\ H] = [20, 120, 80]$μm shown in Fig. 2a. The vapor bubble expands rapidly and reaches the droplet's periphery in 1.32 ms.

Movie S3

Vibration jumping droplet on micropillared substrates at 130 °C.

Side-view video of the vibration jumping droplet shown in Fig. 3a. Water droplet of 2 mm in diameter resting on substrate $[D,\ L,\ H] = [20, 120, 20]$μm vibrates with obvious period on the substrate and finally jumps off the substrate.

Movie S4

Vapor bubble expansion process on hot substrate with 20 μm micropillars.

Top-view video of the bubble growth process on substrate $[D,\ L,\ H] = [20, 120, 20]$μm. The bubble expansion process is interrupted by an obvious shrinking process.

Movie S5

Vapor bubble expansion process on hot substrate with 60 μm micropillars.

Top-view video of the bubble growth process on substrate $[D,\ L,\ H] = [20, 120, 60]$μm. The bubble expansion process is interrupted by an obvious shrinking process. And then the bubble expands slowly to cover the droplet base.

Movie S6

Rapid droplet purging process on tilted substrate.

Side-view video of the droplet jumping process on tilted substrates. For the tilted substrate $[D,\ L,\ H] = [20, 120, 20]$ μm, the droplet initiates the out-of-plate jumping via vibration and lands softly on the substrate remaining in the low-friction Cassie state until it slides off the substrate. For the tilted substrate $[D,\ L,\ H] = [20, 120, 80]$ μm, the Leidenfrost-like droplet jumps explosively from the substrate and experiences repetitive rebounding and falling for several cycles before it finally rolls off the substrate.

Movie S7

Surface fouling removal process via boiling droplet.

Top-view video of dislodging and removal of fouling from surface roughness by sliding droplet on tilted substrate $[D,\ L,\ H] = [20, 120, 20]$ μm at 130 °C. The initial Wenzel state droplet catches the contaminants in cavities and then the generation of vapor bubbles effectively dislodges the residual contaminant particles and drives them to suspend in the droplet. Finally, the sliding droplet effectively purges the surface fouling.

Reference

1. Korhonen JT, Huhtamäki T, Ikkala O, Ras RH. Reliable measurement of the receding contact angle. *Langmuir* 2013, **29**(12)**:** 3858-3863.